MBE growth of a novel chalcopyrite-type ternary compound $MnGeP_2$

K. Sato, T. Ishibashi, K. Minami, H. Yuasa. J. Jogo, T. Nagatuka, Y. Kangawa and A. Koukitu

Graduate School of Engineering, Tokyo University of Agriculture and Technology, Tokyo 184-8588, Japan

Abstract

Novel ternary Mn-containing compound $MnGeP_2$ has been grown on GaAs and InP substrates using molecular beam epitaxy, in which Mn and Ge were supplied from solid sources and P from a gas source. The films obtained showed XRD pattern characteristic of $MnGeP_2$. Lattice constants were determined using reciprocal lattice mapping analysis. Films directly grown on GaAs substrate showed three-dimensional grain-growth. By introduction of a Ge buffer layer growth mode became two-dimensional. The magnetization vs. temperature curve showed ferromagnetic properties at room temperature. Magneto-optical spectra showed a structure around 2 eV.

Keywords: magnetic semiconductor, chalcopyrite type structure, manganese germanium di-phosphide, molecular beam epitaxy

1. Introduction

We have been working with chalcopyrite type compounds doped with transition elements.[1-3] In the course of the study, we discovered novel room-temperature ferromagnetic semiconductors based on the chalcopyrite-type compounds by doping high concentration of Mn to the surface region of $CdGeP_2$ and $ZnGeP_2$ bulk single crystals.[4-8] The physical origin of ferromagnetism is still in controversy.[9-11] Room-temperature ferromagnetism reported in $ZnGeP_2$:Mn by Cho et al.[12] was attributed afterwards to segregation of MnP phase by NMR studies, even though the amount of the phase being less than the detection limit by X-ray diffraction (XRD),[13] indicating a crucial importance of careful material preparation.

We have performed *in-situ* X-ray photoelectron spectroscopy (XPS) observation during Mn deposition on $ZnGeP_2$ crystal and during sputter-etching after Mn was deposited at elevated temperatures,[14] from which it has been revealed that Mn completely occupies the Zn site in the surface region of the host crystal and the Mn^{2+} states characteristic of the diluted magnetic semiconductor is buried in the depth of a few tens of nm from the surface. It is thus clear that the material has an inhomogeneous distribution of Mn species toward depth direction; i.e., the top surface is covered by a Mn-Ge-P compound and ferromagnetic layer is buried under the surface. In addition, we postulate that the Mn-Ge-P compound should have a chalcopyrite-analogous crystal structure, since the chalcopyrite structure seems to be sustained throughout the Mn-deposition process since the reflection high energy electron diffraction (RHEED) show streak pattern that can be assigned to chalcopyrite phase.[7].

Therefore it is important to prepare single-phase compound in which Mn is doped homogeneously. For this purpose we employed molecular beam epitaxy (MBE) technique, which is capable of controlling compositions precisely. As one step for an approach to the $Cd_{1-x}Mn_xGeP_2$ system, we started with the concentrated limit; i.e., $MnGeP_2$.

An existence of novel chalcopyrite-type $MnGeP_2$ was first predicted by a theoretical studies by Mahadevan and Zunger, suggesting the material is antiferromagnetic.[10] Recently, Cho et al. reported preparation of $MnGeP_2$ polycrystalline crystals and thin films, indicating that these films show ferromagnetism at room temperature.[15] However, they showed no detailed description on crystallographic properties of thin films. Therefore it is meaningful to prepare $MnGeP_2$ thin films with well-defined crystallographic properties by an MBE technique.

Prior to the MBE growth we carried out ab-initio calculation to estimate a stability of the ternary compounds in MnP-GeP pseudo-binary system, and confirmed stable existence of chalcopyrite phase of $MnGeP_2$.

2. Ab-initio Calculation

Prior to experimental studies, we examined formation of $MnGeP_2$ using $DMOL^3$ code, i.e., density functional theory for molecules and three-dimensional periodic solids. [16] $DMOL^3$ has been successfully applied to band-structure calculations of insulating and metallic solids and the complex structure of the $BaTiO_3$ grain boundary.[17] In this work, localized numerical orbitals were used as basis set, where a double set of numerical valence functions with a local basis cut-off Rc=5.5Å was used. The relativistic treatments for the atoms are done via a pseudopotential [18] acting on all-electrons, including core, to get scalar relativistic corrections for the relevant valence orbitals. The generalized gradient approximation (GGA) functional of Perdew-Burke-Ernzerhof [19] is used to illustrate the dependence of our theoretical predictions on functional treatments.

Figure 1 shows calculated enthalpy of mixing as a function of solid composition x of Mn in $Mn_xGe_{1-x}P$. In

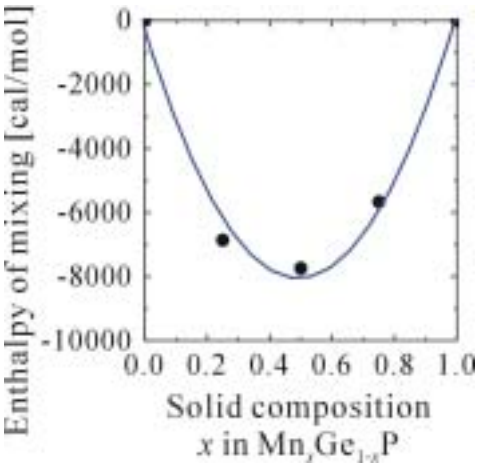

Fig. 1 Enthalpy of mixing calculated in MnP-GeP system

this calculation, MnP and GeP (*i.e.*, the case of x=1.0 and 0.0) are assumed to have a zincblende (ZB) structure because ZB type of transition atom-related compounds such as CrAs[20] and MnAs[21] have been known to grow on GaAs substrates. The calculated results suggest that the chalcopyrite phase with x=0.5 is the most stable state and should exist although the lattice constraint from the substrates should have been incorporated to predict the detailed thermodynamic properties of thin films.

3. Experiments

The MBE apparatus used for this study was equipped with Knudsen cells for Mn and Ge evaporation, and a cracking cell for decomposing tertiary butyl phosphine (TBP) to supply P_2 gas, the flow rate of which is controlled by a mass flow controller. The cracking cell was designed following the work reported by H. Sai et al. [22]. The temperature of the cracking cell is kept at 810~835^{o}C to assure an efficient decomposition of TPB into P_2 during the MBE growth [23].

As substrates we employed GaAs (001) and InP (001) single crystal wafers. Surface treatments of substrates were performed as follows: The GaAs (001) substrate was treated by a H_2O_2+NH_3+H_2O (1:3:50) solution, while no etching process was applied to InP (001) "epi-ready" wafers. Thermal cleaning of GaAs substrates was performed at 580^{o}C in vacuum (~10^{-8} Torr) without As and that of InP at 480^{o}C in a P_2-flow. The growth process was monitored using an in-situ RHEED measurement.

The surface morphology was observed by a scanning electron microscope (SEM). Chemical compositions were measured using an energy-dispersive X-ray analysis (EDX) attached to the SEM apparatus. The crystals were analyzed by X-ray diffraction (XRD) technique using an X-ray diffractometer (Philips type X'Pert). Temperature-dependence of magnetization was measured by a SQUID magnetometer. Magneto-optical spectra were measured at room temperature using a specially designed magneto-optical spectrometer using an optical retardation modulation technique.[24]

4. Results and discussion

4.1 Growth of $MnGeP_2$ on GaAs(001) and InP(001) substrates [25]

Growth conditions of thin films prepared in the present study and chemical compositions of these films measured by EDX are summarized in Tables 1 and 2. GaAs(001) substrates were used for samples #1 to #4 shown in Table 1, while InP(001) substrates were used for samples #5 to #8 shown in Table 2. The beam equivalent pressure (BEP) of both Mn and Ge was varied between 6.4×10^{-9} and 9×10^{-9} Torr. The values of BEP for Mn and Ge were adjusted to take the same value, since the sticking coefficient of Mn and Ge was found to have the same value from our preliminary experiments. The TBP flow rate was set to be between 1.6 and 2.0 sccm. Substrate temperatures of 342 - 541^{o}C were used and deposition time was 90 - 180 minutes.

The composition ratio of Mn/Ge listed in the last columns in Tables 1 and 2 was deviated from 1 because of a difficulty in adjustment of the low beam fluxes of 10^{-9} – 10^{-8} Torr. In all cases, no re-evaporation of Mn was confirmed within an experimental error. We could not determine an exact value of the partial pressure of P_2 in our MBE system, but it should be several orders of magnitude higher than Mn and Ge, taking into account the total pressure reaching as high as 10^{-4} Torr during growth.

Figures 2 and 3 show XRD patterns measured in the samples shown in Tables 1 and 2, respectively. It is found that diffraction line due to zinc-blend (ZB) type GeP [26] are observed in the samples #1 and #2 which were prepared at high growth rate using flux rate of Mn and Ge exceeding 1.8×10^{-8} Torr. In contrast, GeP can not be detected by XRD measurements when the beam fluxes of Mn and Ge is lower than 1.1×10^{-8} Torr. The similar feature is observed for MnP.

Although it was quite difficult to completely suppress a segregation of MnP, whose diffraction lines were almost suppressed in films prepared on InP substrates using the low beam flux less than 1×10^{-8} Torr. Suppression of secondary phases has a crucial importance for magnetic studies of $MnGeP_2$, because MnP and Mn_5Ge_3 are known to show ferromagnetism at room temperature.

Table 1 Growth conditions for thin films on GaAs (001) substrates

Sam-ple	Mn flux [10^{-8}Torr]	Ge flux [10^{-8}Torr]	TBP flow rate [sccm]	Tsub [^{o}C]	Time [min]	Composition Mn:Ge:P
#1	1.8	1.8	1.6	541	90	0.81 : 1 : 1.11
#2	2.4	2.1	1.6	414	180	1.72 : 1 : 2.99
#3	1.1	1.1	2.0	400	240	1.37 : 1 : 2.59
#4	0.65	0. 9	2.0	400	180	0.95 : 1 : 2.14

Table 2 Growth conditions for thin films on InP (001) substrates.

Sam-ple	Mn flux [10^{-8}Torr]	Ge flux [10^{-8}Torr]	TBP flow rate [sccm]	Tsub [^{o}C]	Time [min]	Composition Mn:Ge:P
#5	0.9	0.9	2.0	435	180	1.92 : 1 : -
#6	1.0	1.0	2.0	342	180	1.29 : 1 : -
#7	0.65	0.9	2.0	342	100	0.95 : 1 : -
#8	0.64	0.64	2.0	435	180	1.40 : 1 : -

No XRD peaks that can be assigned to $MnGeP_2$ have been observed in Fig. 2 for samples #1 to #4 deposited on GaAs substrates, despite that deposition of Mn, Ge and P atoms were confirmed by EDX in these films. We estimated that the diffraction lines from $MnGeP_2$ are hidden behind the strong 00*l* diffractions from the substrate. To discriminate the XRD line of the film from that of substrate, we changed the substrate from GaAs to InP, the latter having the different lattice constant from GaAs.

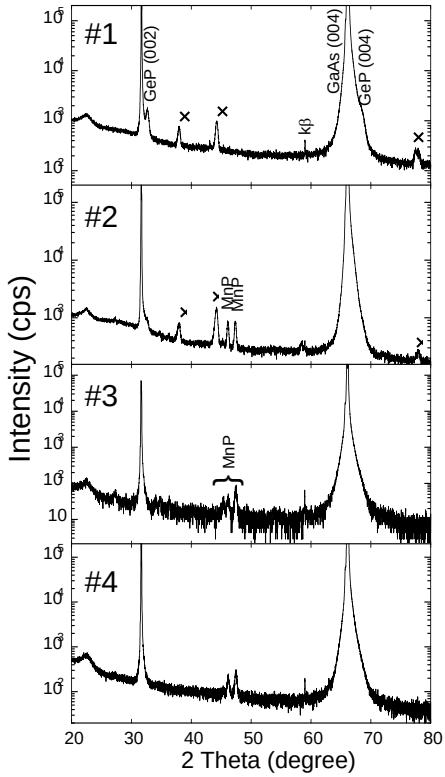

Fig.2 The XRD θ-2θ scan chart of the films on GaAs(001); lines × are due to Al holder

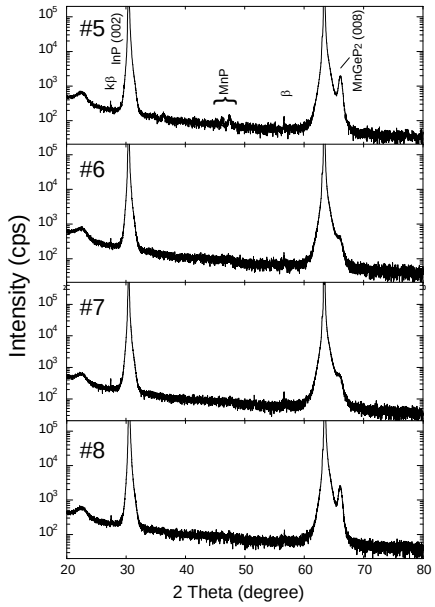

Fig. 3 The XRD θ-2θ scan chart of the films on InP (001)

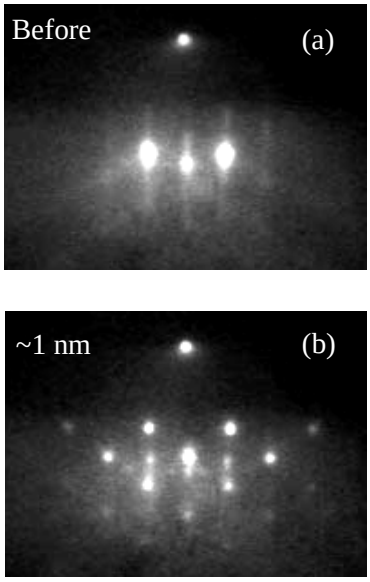

Fig. 4 RHEED pattern taken (a) before and (b) just after deposition

As shown in Fig. 3, the XRD curves of the sample#5-#8 deposited on InP (001) substrates show a diffraction peak at 2θ~66.04° clearly resolved from the 004 diffraction line of the InP substrate. The peak position of the film coincide with the 004 diffraction of GaAs.. The diffraction line is labeled as 008 assuming that the chalcopyrite $MnGeP_2$ is grown with the c-axis perpendicular to the substrate surface. The position of the peak is so close to that of the 004 diffraction of GaAs that it can only be discriminated in films prepared on InP substrates, the lattice constant of the latter being much larger than GaAs.

The XRD peak assigned to 008 reflection from $MnGeP_2$ seems not strong in samples #6 and #7, grown at reduced substrate temperature of 342°C. This means that higher substrate temperature is favorable to get a good crystallinity due to enhanced surface migration of deposited atoms.

Figure 4 shows RHEED patterns of the thin film of sample#4 before and during the growth. The incident

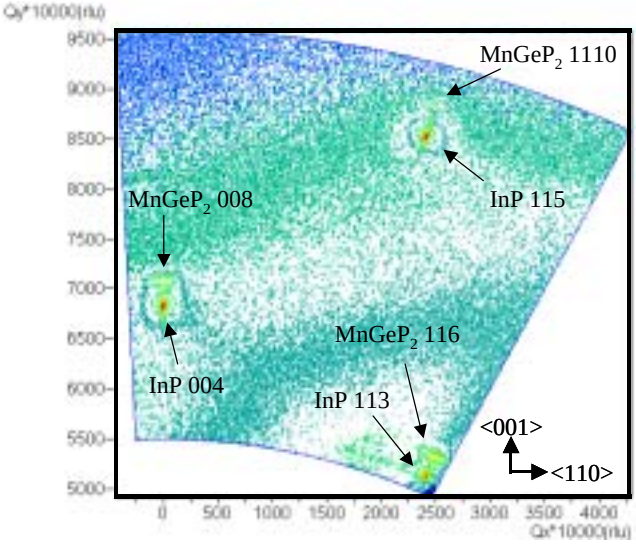

Fig. 5 Reciprocal lattice mapping of XRD from $MnGeP_2$

electron beam was along InP [110] azimuth. Figure 4(a) shows the streaky patterns from the InP substrate before the growth. The streaky patterns completely varied to spotty ones keeping the same spacing as observed at immediately after starting of the growth (Fig.4(b)). This change of RHEED patterns suggests that this film was grown under the 3-dimensional Volmer-Weber or Stranski-Krastanov mode at the initial stage. This consideration is also supported by a SEM image.

4.2 Reciprocal lattice mapping of XRD in $MnGeP_2$ on InP(001) substrates [27]

In order to determine the crystal structure and lattice constants of the sample #8, the X-ray reciprocal lattice mapping (RLM) measurement was carried out. Figure 5 shows the RLM image, which is a part of the plane in the reciprocal lattice space including InP <001> and <110> directions. Horizontal (Q_x) and vertical (Q_y) axes are the reciprocals of the in-plane and the out-of-plane lattice constants, respectively. In this map, $MnGeP_2$ 008, 116, 11 10 diffraction spots close to those of InP 004, 113, 115 were observed and formed pairs, respectively. These pairs of diffraction spots reflected from the substrate and the grown film suggest the orientation relationship as follows: $MnGeP_2$<001>//InP<001> and $MnGeP_2$<110> //InP<110>. Assuming chalcopyrite structure with the tetragonal crystal system, we can determine the lattice constants to be a=5.693 Å and c=11.303 Å, which is consistent with those by the theoretical calculation [9, 28] and with those determined experimentally in the polycrystalline $MnGeP_2$ reported by Cho *et al.*[15]

Table 3 Growth conditions for thin films without and with a Ge-buffer

Sam-ple	buffer	Mn flux 10^{-8} [Torr]	Ge flux 10^{-8}[Torr]	TBP [sccm]	Temp .[°C]	Time [min]	Mn:Ge:P
#9	–	0.6	0.6×	2.0	435	180	1.00:1.04:2.05
#10	Ge	0.6	0.6	2.0	435	180	1.00:–:1.56

4.3 Growth condition of $MnGeP_2$ on a Ge-buffer layer [29]

It is found from our experimental studies that the buffer layer is strongly required to get two-dimensional growth suppressing a formation of secondary phases. We consider that Ge is a good candidate as buffer layer, because it has been known that II-Ge-V_2 chalcopyrites tend to form a solid solution with Ge [30, 31], and the lattice constant of Ge (5.657 Å) is close to both lattice constants of GaAs (5.653 Å) and $MnGeP_2$ [9,15].

Table 3 summarizes growth conditions of $MnGeP_2$ films on GaAs(001) without and with a Ge a buffer layer. Sample #9 was directly grown on GaAs(001), while sample#10 was grown on a Ge buffer layer, the latter having been grown on the GaAs substrate at 380°C. Growth temperature of $MnGeP_2$ was 435°C in both experiments.

Figure 6 shows RHEED patterns of sample #10 taken during the growth. The direction of incident electron beam is along the [110] azimuth of the substrate. Figure 6(a) shows a streak pattern with the 2×2 surface

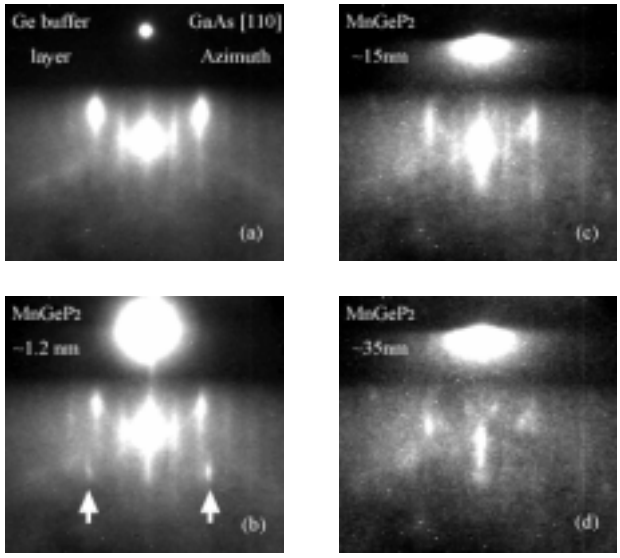

Fig. 6 (a) RHEED patterns of Ge buffer layer grown on a GaAs, and (b)-(d) $MnGeP_2$ film grown on a Ge buffer layer. Azimuth is GaAs[110].

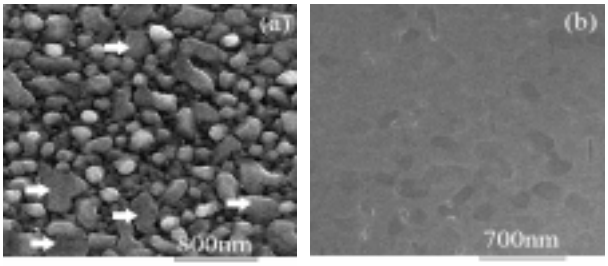

Fig. 7 SEM photographs showing surface morphology in $MnGeP_2$ (a) without a buffer and (b) with a Ge buffer.

reconstruction, indicating that the Ge buffer layer improves the surface flatness. During the growth of $MnGeP_2$, the 2×2 streak pattern was observed until thickness reaches 15 nm as shown in Figs. 6(b) and 6(c). We attribute the 2x2 reconstructions to P-dimmers in $MnGeP_2$ by analogy of the group V dimmers in III-V compounds.

However the segregation of MnP was confirmed in Fig. 6(b) as pointed by arrows, suggesting that an oriented overgrowth of a small amount of MnP also occurred. For the thickness above 35 nm, the surface reconstruction disappeared and some spots related to secondary phases appeared as shown in Fig. 6(d).

As shown in Fig. 7(a), the sample #9 shows a rough surface morphology in which the grains with a flat surface pointed by arrows may be assigned to $MnGeP_2$ and the other small grains to secondary phases. On the other hand, the surface morphology of the film on the Ge buffer layer is very flat as shown in Fig. 7(b)..

The two-dimensional growth of $MnGeP_2$ may be explained by an enhanced migration of Mn and Ge atoms due to improved flatness of the surface by introduction of the Ge buffer layer. In addition we consider that the crystallographic affinity between $MnGeP_2$ and Ge may further assist the crystal growth. As stated above, our films suffer segregation of secondary phase (MnP) even though the film composition was nearly stoichiometric. In order to obtain single phase $MnGeP_2$ crystal, we are

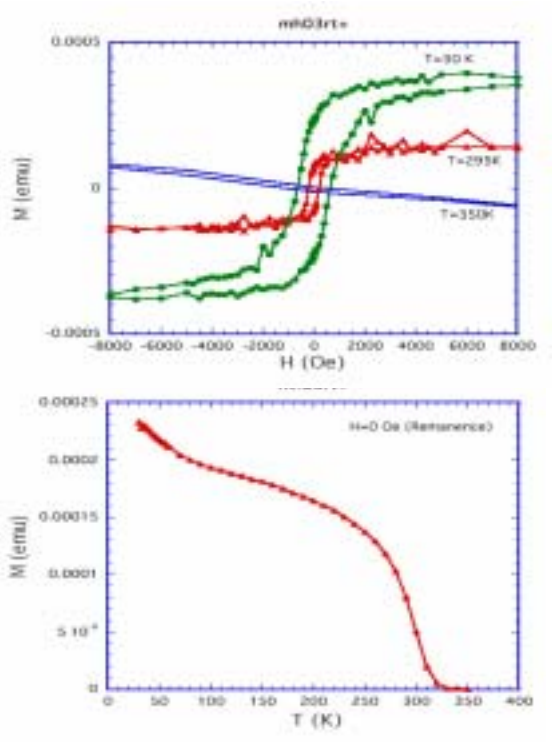

Fig. 8 Magnetic properties in $MnGeP_2$/InP(001) (sample #6) , (a) M-H curves at 30 K, 295 K, 350 K, and (b) an M-T curve measured at remanence.

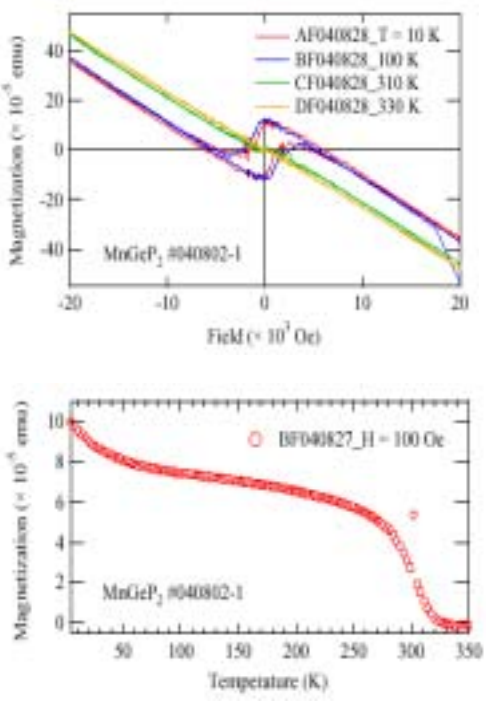

Fig. 9 Magnetic properties of $MnGeP_2$ /Ge/GaAs (sample #10)film; (a) M-H, (b) M-T curves measured with H=100 Oe.

performing the thermodynamic calculation in MnP-GeP system. A preliminary result suggests that growth temperature above 700°C with reduced Mn/(Mn+Ge) ratio favors a formation of $MnGeP_2$ suppressing secondary phases. [32] Experimental studies to obtain an optimal growth condition are underway.

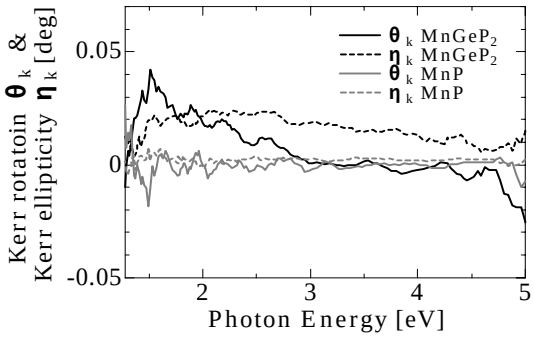

Fig. 10 Magneto-optical Kerr rotation θ_K (solid black line) and ellipticity (dotted black line) spectrum in $MnGeP_2$ on Ge buffer (sample#10) For reference θ_K and η_K in MnP are plotted by gray lines

4.4 Magnetic and magneto-optical characterization

Figure 8(a) shows typical hysteresis curves measured at 30 K, 295 K and 350 K in a $MnGeP_2$ film grown on the InP(001) substrate (Sample #6). The temperature dependence curve of magnetization measured at the remanent state is plotted in Fig. 8(b), from which Curie temperature Tc of 320 K is deduced.

Figures 9(a) and 9(b) are M-H and M-T curves of $MnGeP_2$ grown on Ge-buffer, which are very similar to those of $MnGeP_2$ on InP(001). The Curie temperature of this sample is also 320 K. The Tc value in both samples is much higher than that of orthorhombic MnP which shows Tc=292 K. The saturation magnetization shows a very small value of about 40 emu/cm^3. Assuming that $MnGeP_2$ crystallizes in chalcopyrite structure with lattice constants a=0.569nm and c=1.130nm, magnetic moment per Mn atom is estimated to be as small as about 0.1μ_B. This value is rather reasonable for $MnGeP_2$, since theoretical study predicted antiferromagnetism with sublattice moment of 0.25 μ_B per Mn.[10] According to the theoretical approach by Kamatani and Akai, the ferromagnetic moment may be originated from disorder in the atomic arrangement or some kind of intrinsic defects.[11] However, at the present stage we cannot completely exclude a possibility that the observed ferromagnetic property comes from some secondary phases, since RHEED pattern clearly exhibit a trace of a MnP-like phase.

Spectra of magneto-optical Kerr rotation and ellipticity were measured at room temperature (about 300K) in $MnGeP_2$ film deposited on Ge buffer layer (sample #10), together with those in MnP film on Ge buffer. It is clear MnP film does not show any appreciable magneto-optical effect, while well-defined spectra were observed in $MnGeP_2$ film, although the peak values of the magneto-optical effect were small. Kerr rotation peak was located at 1.5 eV with the value of approximately 0.04°. Lack of magneto-optical effect in MnP may be explained by the fact that ambient temperature is above Tc(=292 K). We also measured optical reflectivity spectra. Spectral feature of reflectivity spectrum in $MnGeP_2$ is completely different from that of MnP. We therefore conclude that the magneto-optical

(a) (b)

effect of sample #10 is not resulting from MnP compound, but from $MnGeP_2$.

5. Conclusion

Novel ternary Mn-containing compound $MnGeP_2$ has been grown using MBE technique. The crystal structure and lattice constants were determined. The material shows ferromagnetism and magneto-optical effect at room temperature.

Acknowledgements

This work has been carried out under the 21st COE Project “Future Nano Materials” of TUAT and supported in part by the Grant-in-Aid for Scientific Research (A) (1) (Category Number:13305003) from Japan Society for the Promotion of Science. We sincerely thank Prof. K. Takanashi of Tohoku University and Prof. A. Fujimori of University of Tokyo for their help in magnetic measurements.

1. K. Sato, H. Tsunoda and T. Teranishi, *Proc. 7th Int. Conf. Ternary and Multinary Compounds, Snowmass, 1986* (Mater. Res. Soc., Pittsburg, 1987) 459.
2. K. Sato, I. Aksenov, N. Nishikawa and T. Kai, *Proc. 9th Int. Conf. Ternary & Multinary Compounds, Yokohama, August 1993* , Jpn. J. Appl. Phys. **32**, (1993) Suppl. 32-3, pp. 481.
3. K. Sato, *Japanese Research Review for Pioneering Ternary and Multinary Compounds in the 21st Century,* eds. by T. Matsumoto, T.Takizawa, S. Shirakata, T. Wada and N. Yamamoto, (IPAP, Tokyo, 2001) 228.
4. G. A Medvedkin, T. Ishibashi, T. Nishi, K .Hayata, Y. Hasegawa and K. Sato, Jpn. J. Appl. Phys. **39** (2000) L949.
5. G.A. Medvedkin, K. Hirose, T. Ishibashi, T. Nishi, V.G. Voevodin and K. Sato, J. Cryst. Growth **236** (2002) 609.
6. K. Sato, G. A. Medvedkin , T. Nishi, Y.i Hasegawa, R. Misawa, K. Hirose and T. Ishibashi, J. Appl. Phys. **88** (2001) 7027.
7. K. Sato, G.A. Medvedkin and T. Ishibashi: J. Crystal Growth **237-239** (2002) 1363.
8. K. Sato, G.A. Medvedkin, T. Ishibashi, S. Mitani, K. Takanashi, Y. Ishida, D.D. Sarma, J. Okabayashi, A. Fujimori, T. Kamatani, H. Akai: J. Phys. Chem. Solids **64** (2003) 1461.
9. Y.-J. Zhao, W. T. Geng, .A. J. Freeman and T. Oguchi: Phys. Rev. **B63** (2001) 201202 (R)
10. P. Mahadevan and A. Zunger, Phys. Rev. Lett. **88** (2002) 047205
11. K. Kamatani and H. Akai, Phase Transitions **76** (2003) 401.
12. S. Cho,.S. Choi, G.-B. Cha, S. C. Hong, Y. Kim, Y.-J. Zhao, A. J. Freeman, J. B. Ketterson, B. J. Kim, Y. C. Kim, B.-C. Choi, Phys. Rev. Lett. **88** (2002) 257203.
13. T. Hwang, J.-H. Shim, and S. Lee, Appl. Phys. Lett. **83** (2003) 1809.
14. Y. Ishida, D.D. Sarma, K. Okazaki, J. Okabayashi, J.I. Hwang, H. Ott, A. Fujimori, G.A. Medvedkin, T. Ishibashi and K. Sato, Phys. Rev. Lett. **91** (2003) 107202.
15. S.Cho, S. Choi, G.-B. Cha, S.C. Hong, Y. Kim, A.J. Freeman, J.B. Ketterson, Y. Park, H.-M. Park; Solid State Commun..**129** (2004) 609.
16. B. Delley, J. Chem. Phys. **113** (2000) 7756.
17. B. Delley, J. Chem. Phys. **92** (1990) 508.
18. B. Delley, Int. J. Quantum Chem. **69** (1998) 423.
19. J. P. Perdew, K. Burke and M. Ernzehof, Phys. Rev. Lett. **77** (1996) 3865.
20. H. Akinaga, T.Manago, and M.Shirai, Jpn. J. Appl. Phys. **39** Part2 (2000) L1118.
21. K. Ono, J. Okabayashi, M. Mizuguchi, M. Oshima, A.Fujimori, H. Akinaga; J. Appl. Phys. **91** (2002) 8088.
22. H. Sai, H. Fujikura and H. Hasegawa, Jpn. J. Appl. Phys. **38**, Part 2 (1999) 151.
23. E. A. Beam, III , T. S. Henderson, A. C. Seabaugh and J. Y. Yang, J. Crystal Growth **116** (1992) 436.
24. K. Sato, H. Hongu, H. Ikekame, Y. Tosaka, M. Watanabe, K. Takanashi and H. Fujimori, Jpn. J. Appl. Phys. **32** Part 1 (1993) 989.
25. T. Ishibashi, K. Minami, J. Jogo, T. Nagatsuka, H. Yuasa, V. Smirnov, Y. Kangawa, A. Koukitu and K. Sato, *Proc. The 3rd International Conference on Physics and Applications of Spin-Related Phenomena in Semiconductors* (*PASPSIII*), J. Superconductivity: Incorporating Novel Magnetism (JOSC) (in press).
26. JCPDS-ICDD No.#210353
27. K. Minami, J. Jogo, V. Smirnov, H. Yuasa, T. Nagatsuka, T. Ishibashi, Y. Morishita Y. Matsuo, Y. Kangawa, A. Koukitu and K. Sato, submitted to Jpn. J. Appl. Phys. Part 2.
28. Y.-J. Zhao, S. Picozzi, A. Continenza, W.T. Geng, A.J. Freeman, Phys. Rev B. **65** (2002) 094415.
29. K. Minami, J. Jogo, Y. Morishita, T. Ishibashi and K. Sato, submitted to Proc. Int. Conf. MBE, *J. Cryst. Growth*.
30. A.S. Borshchevskii, N.A. Goryunova, F.P. Kesamanly, and D.N.Nasledov, Phys. Stat. Sol. **21** (1967) 9.
31. G. C. Xing, K.J Bachman, G.S. Solomon, J.B. Posthill, M.L. Timmons, J. Cryst. Growth **94** (1989) 381.
32. Y. Kangawa: private communication.